A two-species model of aeolian sand transport

By B R U N O   A N D R E O T T I

Laboratoire de Physique Statistique de l'E. N. S., 24 rue Lhomond, F-75005 Paris, France
Matière et Systèmes Complexes, rue Watt, F-75013 Paris, France

The transport of sand by wind results from the equilibrium between the erosion of grains dragged by the flow and the resulting slow down of the wind velocity. The dynamical mechanisms governing the saturation of the sand flux are investigated theoretically. We first demonstrate that previous models, based on the assumption that all the grains have the same trajectory, are either not self-consistent or lead to unstable solutions. A model based on a discrete number of states is derived, which solves these problems. Two well-defined species of grain appear, which correspond to saltons (high-energy grains) and reptons (grains ejected from the sand bed by the impact of saltons). They play specific roles: the negative feedback of the transport on the wind is limited to the reptation layer while most of the transport is due to saltation. The model is further simplified, benefiting from the existence of these two species and the dependencies of the threshold velocity, the saturated flux, the aerodynamic roughness and the saturation length are derived and compared to experimental measurements.

1. Introduction

The morphogenesis and the dynamics of dunes is controlled by the transport of sand by the wind (Bagnold 1941). The shape of the dune determines the velocity field around it. In turn, the wind controls the sand flux and thus modifies the dune topography through the erosion/deposition process. The flux of sand which can be transported by a given wind is limited to an equilibrium value called the saturated flux, which increases with the wind strength. There has been a great effort to obtain experimentally (Chepil & Milne 1939; Bagnold 1941; Zingg 1953; Williams 1964; Svasek & Terwindt 1974; Nickling 1978; Jones & Willetts 1979; White 1979; Willetts, Rice & Swaine 1982; Greeley, Blumberg & Williams 1996; Iversen & Rasmussen 1999) using both wind tunnels and atmospheric flows on the field, numerically (Anderson & Haff 1988, 1991; Werner 1990) and theoretically (Bagnold 1941; Kawamura 1951; Owen 1964; Kind 1976; Lettau & Lettau 1978; Ungar & Haff 1987; Sørensen 1991; Sauermann, Kroy & Herrmann 2001), the relationship between the saturated flux over a flat sand bed and the shear velocity u_*. Apart from the work by Ungar & Haff (1987) which we shall turn to later, all the theoretical studies give similar results: the saturated flux q vanishes below a threshold value u_{th} of the shear velocity and scales at large shear velocity like the Bagnold (1941) prediction,

$$q_B = \frac{\rho_{\mathrm{air}} u_*^3}{g} \qquad (1.1)$$

where ρ_{air} is the density of air.

Although there are a large number of previous studies and some of these models fit the experimental data well (Iversen & Rasmussen 1999), we wish here to investigate the sand transport problem again, aiming to focus on the dynamical mechanisms responsible for its saturation. In this introduction, we will show that all previous theoretical works are either not self-consistent or correspond to unstable solutions. The problem arises because the previous models (Bagnold 1941; Kawamura 1951; Owen 1964; Kind 1976; Lettau & Lettau 1978; Ungar & Haff 1987; Sørensen 1991; Sauermann et al. 2001) assume that 'the entire particulate motion, which in reality must be endowed with a certain randomness, is regarded as repetitive such that the trajectory shape of one particle is identical with that of any other' (Owen 1964, p. 226). We will show in this paper that two types of trajectory have to be considered simultaneously in order to recover the missing properties.

The first steps of the saturation process have been observed by Willetts, McEwan & Rice (1991) and studied numerically by Anderson & Haff (1988, 1991). The first few grains in motion are directly dislodged and dragged by the fluid. These grains in 'tractation' roll at the surface (Willetts et al. 1991; Andreotti, Claudin & Douady 2002a) until they take off, owing to the bumps beneath them or to the aerodynamic lift force. Once the sand transport is initiated, a second more efficient mechanism, takes over from tractation. When the hopping grains collide with the bed, they eject other grains. The latter are accelerated by the wind, splash up other grains and so on. In this second step, there is thus an exponential increase of the sand flux. Those grains which have sufficient energy to eject other grains from the sand bed are said to be in 'saltation'. The low-energy grains ejected are said to be in 'reptation' (Anderson, Sørensen & Willetts 1991). To pun on the name of particles in solid state physics, Andreotti et al. (2002a) have proposed calling saltons the grains in saltation, reptons the grains in reptation and tractons the grains in tractation. Note that saltons, tractons and reptons are not different in nature, but only in their energy. In the last step, the sand flux saturates, owing to the negative feedback of the sand transport on the wind strength; if the wind accelerates the grains, the latter exert a further stress on the air. The saturated transport corresponds to the equilibrium state of the turbulent boundary layer between the driving by upper atmospheric layers and the friction due to both the turbulent motion and the drag of the grains.

To point out the paradox of the one-species models, we recall the basic assumptions and the predictions of the model established by Owen (1964) as it is the reference of the others. Consider that a large number of grains are dragged by the wind but that they have strictly identical trajectories. The sand transport is characterized by the flux q which is the mass of grains which crosses a unit length perpendicular to the wind stream per unit time (figure 1). The term q is the flux measured when vertical sand traps are used. If a horizontal sand trap buried in the sand is used, we measure the vertical flux ϕ which is the mass of particles colliding with the soil per unit time and unit area. Since q is a linear flux and ϕ a surface flux, the ratio of the two is a length. It can easily be inferred from figure 1 that this length is exactly the grain hop length L:

$$q = \phi L. \qquad (1.2)$$

Since they are accelerated by the wind, the grains, at a height z, have a smaller horizontal velocity $v_\uparrow(z)$ when they go up than when they come down again, $v_\downarrow(z)$ (figure 1). Since all the trajectories are assumed to be identical, the mass of particles crossing the altitude z per unit time and unit area is equal to ϕ, provided that z is smaller than the hop height H. It is zero above the saltation layer ($z > H$). As shown
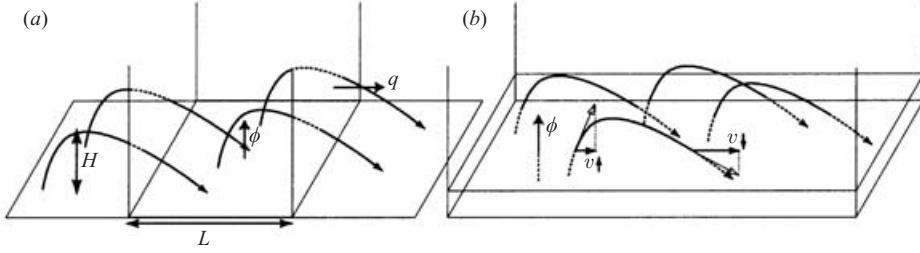
FIGURE 1. (*a*) The flux q is the mass of sand which crosses a unit line transverse to the wind per unit time. If the path of the grains has a length L, the incident flux of grains ϕ, which is the mass of grains colliding with a unit area per unit time, is equal to q/L. (*b*) If the trajectories are assumed to be identical (one-species assumption), ϕ is also the mass flux through any horizontal slice lower than H. The sand-borne shear stress τ_{sand} is equal to the flux of horizontal momentum through this slice, i.e. to the difference between the downward flux $\phi v_\downarrow$ and the upward flux $\phi v_\uparrow$.

by Bagnold (1941), the transfer of momentum from the air to these grains is simply the mass flux ϕ multiplied by the velocity difference $v_\downarrow - v_\uparrow$:

$$\tau_{sand} = \phi(v_\downarrow - v_\uparrow). \tag{1.3}$$

The remaining part of the total shear stress, the air-borne shear stress $\tau_{air} = \tau_0 - \tau_{sand}$, accelerates the air flow itself. Now, the flux saturates when 'the shearing stress borne by the fluid falls, as the surface is approached, to a value just sufficient to ensure that the surface grains are in a mobile state' (Owen 1964, p. 226). This can be put in a formal way by requiring that $\tau_{air} = \rho_{air} u_{th}^2$ at the surface of the sand bed whatever the wind strength. The expression of the flux follows as:

$$q = \rho_{air}\left(u_*^2 - u_{th}^2\right)\frac{L}{v_\downarrow - v_\uparrow}. \tag{1.4}$$

To close the model, we have to determine the unique trajectory and deduce L and $v_\downarrow - v_\uparrow$. The different propositions for this saltation trajectory have led to the different one-species models previously cited (see Iversen & Rasmussen 1999 for a summary). Those proposed by Bagnold (1941), Kawamura (1951), Kind (1976), Lettau & Lettau (1978), Sørensen (1991) and Sauermann *et al.* (2001) have the same physical basis as that of Owen (1964). We will thus limit ourselves to analysing two models of different natures: Owen (1964) and Ungar & Haff (1987).

It is reasonable to assume that the velocity difference $v_\downarrow - v_\uparrow$ scales on the mean horizontal velocity so that the ratio $L/(v_\downarrow - v_\uparrow)$ scales on the hop time T. Equation (1.4) becomes:

$$q \propto \rho_{air}\left(u_*^2 - u_{th}^2\right)T. \tag{1.5}$$

At this step, we usually assume that the grains are submitted to a wind velocity scaling as u_*. In the limit where gravity is much larger than the vertical component of the drag, T scales as u_*/g (Bagnold 1941; Kind 1976). In the other limit of an important vertical drag, most of the time, the vertical velocity is the fall velocity u_{fall} that results from the balance between gravity and fluid drag. The Owen (1964) model is a mix of the two:

$$q_O = \rho_{air}\left(u_*^2 - u_{th}^2\right)\frac{\alpha u_{fall} + \beta u_*}{g}. \tag{1.6}$$

From the point of view of dynamical mechanisms, Owen's picture can be summarized as follows. Equilibrium is reached when the fluid shear inside the saltation curtain is decreased to the value for which grain dislodgement is just possible, i.e. to the threshold value. Outside the saltation curtain, the sand flux and thus the sand-borne shear stress vanishes: the shear velocity remains equal to u_* for $z > H$. The wind velocity is strongly reduced for $z < H$ so that the saltation curtain should behave as an aerodynamic roughness z_0 whose height is of the order of the layer thickness H; but all the experiments (Bagnold 1941; Zingg 1953; Rasmussen, Iversen & Rautaheimo 1996) have shown that z_0 is much smaller than H (few millimetres compared to tens of centimetres). This means that the wind is almost undisturbed at heights larger than, say, 1 cm from the sand bed, as confirmed by common observation. The second argument is due to Ungar & Haff (1987) and points out a problem of self-consistency. We cannot assume that the wind velocity is strongly reduced on the one hand and compute the grain trajectory as if the wind was not disturbed on the other hand. If the friction velocity inside the saltation layer is constant whatever u_*, so should be the trajectory of the grains. In other words, T is not the flight time of grains submitted to the undisturbed wind, but that submitted to a reduced constant wind. As a conclusion, the one-species model by Owen (1964) and those of the same type (Bagnold 1941; Kawamura 1951; Kind 1976; Lettau & Lettau 1978; Sørensen 1991; Sauermann *et al.* 2001) are not self-consistent and thus have to be rejected.

Most of the grains mobilized are ejected by saltons colliding with the sand bed. The characteristics of these ejecta have been investigated numerically by Werner (1988) and Anderson & Haff (1988, 1991) and experimentally by McEwan, Willetts & Rice (1992) and Rioual, Valance & Bideau (2000). They found that the ejection velocity was, statistically, independent of the impact velocity v_{imp}. Since the air is not involved in the ejection process, the ejection velocity should scale on $\sqrt{gd}$ which can be interpreted as the velocity necessary to escape from the potential trapping at the surface of the sand bed (Quartier *et al.* 2000; Andreotti *et al.* 2002a). Similarly, the average number of reptons produced by an impacting salton should be a function of $v_{\mathrm{imp}}/\sqrt{gd}$. Following Ungar & Haff (1987), the saturation occurs when the wind velocity has so decreased that the grains eject no other grains during the collisions with the soil. This means that the impact velocity of the saltons at saturation should scale as $\sqrt{gd}$ whatever the friction velocity u_*. The hop height H and the hop length L should then scale on the grain diameter d and the flight time T on $\sqrt{d/g}$. Equation (1.5) remains valid and predicts:

$$q_{UH} \propto \rho_{\mathrm{air}}\left(u_*^2 - u_{\mathrm{th}}^2\right)\sqrt{\frac{d}{g}}. \tag{1.7}$$

As a conclusion, the unique self-consistent solution to the one species problem is that given by Ungar & Haff (1987). Still, this is not satisfying for two reasons. First, it predicts – assumes? – that all the grains participating to the saturated sand transport are in reptation, i.e. with trajectories of the size of a few grain diameters whatever the wind strength. In fact, many saltons are observed experimentally, making long flights, which could participate in and even dominate the sand transport. If saltation remains at saturation then what makes the flux saturate? Secondly, it is an unstable solution. Suppose that one grain has a slightly higher velocity than the others so that it bounces higher than H. Around the maximum of its trajectory, it enters the undisturbed region of the turbulent boundary layer and is thus accelerated. It thus bounces even higher and so on (of course a new equilibrium trajectory is ultimately

reached, but it depends on the wind strength). This means that the uniform reptation layer is unstable towards the promotion of grains to saltation. As a conclusion, the one-species models are either not self-consistent or unstable.

So, the assumption of a single trajectory should be relaxed. This was done in the numerical simulations by Anderson & Haff (1988, 1991) and Werner (1990) where a continuous distribution of trajectories was investigated. These models seem realistic, but they are too complicated to examine the dynamical mechanisms and they are too heavy to investigate the effect of the numerous parameters. In particular, they introduce a continuous distribution – the so-called splash function – to describe statistically the rebound of one grain. Our strategy here is to remain between the one-species models that do not have good ingredients and the continuous statistical models that are too complicated: we wish to build the simplest *deterministic* model allowing several trajectories. We shall turn later to Anderson & Haff (1988, 1991) and Werner (1990) in order to determine the importance of randomness in the sand transport process. Finally, we wish to emphasize that the concern of the present paper is the dynamical mechanisms governing the saturation of sand transport. In building a new model, we will thus systematically prefer simplicity to realism.

2. The n-generations model

2.1. *Motion of the particles*

Without loss of generality, we can choose the grain diameter d as the unit length and $\sqrt{d/g}$ as the unit time. In order to simplify the discussion, we will consider that the Reynolds number based on the grain size is sufficiently large to consider that the drag is turbulent. In practice, this means that the results will not depend on air viscosity so there are only two control parameters: the wind velocity rescaled by $\sqrt{gd}$ and the grain to fluid density ratio $\rho_{\mathrm{sand}}/\rho_{\mathrm{air}}$.

Once it has left the sand bed, the grain is submitted to the fluid drag force and to gravity. Whatever the shape of the grain, Bagnold (1941) has suggested that the drag force should have the same dependence as that on a rough sphere of effective diameter d. Lift and inertial forces are related to the spatial variations of the wind velocity. So, they are typically of the order of d/H times the drag force and can thus be neglected in first approximation. The mass of the grain is $\rho_{\mathrm{sand}}\pi d^3/6$; introducing the usual drag coefficient C_D, the drag force reads

$$\boldsymbol{f} = \tfrac{1}{8}\rho_{\mathrm{air}}C_D\pi d^2|\boldsymbol{u}-\boldsymbol{v}|(\boldsymbol{u}-\boldsymbol{v}),$$

where $\boldsymbol{v}$ is the grain velocity and $\boldsymbol{u}$ the local wind velocity. Then, the equation of motion reads:

$$\frac{\mathrm{d}\boldsymbol{v}}{\mathrm{d}t} = \boldsymbol{g} + \tfrac{3}{4}C_D\frac{\rho_{\mathrm{air}}}{\rho_{\mathrm{sand}}}\frac{|\boldsymbol{u}-\boldsymbol{v}|(\boldsymbol{u}-\boldsymbol{v})}{d}. \tag{2.1}$$

Being turbulent, the fluid drag varies as the square of the grain speed so that the motion in the horizontal x and vertical z directions are coupled through the velocity difference $|\boldsymbol{u}-\boldsymbol{v}|$.

At this step, we need to fix some laws for the rebound and the ejection processes. When the grain collides with the sand bed, it can rebound, keeping a part of its energy, or remain trapped by the soil. Experiments (McEwan *et al.* 1992; Nalpanis, Hunt & Barrett 1993; Rioual *et al.* 2000) and numerical simulations (Werner 1988; Anderson & Haff 1988, 1991) show that the rebound velocity v_{reb} is, on average, a

fraction of the impact velocity v_{imp}:

$$v_{\mathrm{reb}} = \gamma\, v_{\mathrm{imp}}. \qquad (2.2)$$

The rebound angle θ_{reb} turns out to be almost independent of the impact velocity (modulus and angle). This behaviour is very different from the rebound of a ball on a plane smooth floor. With a specular rebound law ($\theta_{\mathrm{reb}} = \theta_{\mathrm{imp}}$), the hop height would only decay so that there would be no sand transport. The grain actually collides with the sand bed which is composed of many grains in permanent contact. The latter induces a redistribution of the horizontal momentum in the vertical direction which allows the grain to make higher and higher hops. Note that this redistribution exists only when the condition $\sin\theta_{\mathrm{imp}} \leqslant \gamma \sin\theta_{\mathrm{reb}}$ is fulfilled. There are actually large fluctuations of the rebound velocity, but we choose here to keep a deterministic rebound law that corresponds to the mean case. Later, we shall compare our results to the numerical computations by Anderson & Haff (1988, 1991) and Werner (1990) in which a probabilistic splash function is used. Still, we will consider that some of the grains remain trapped at each rebound. As the air is not involved in the rebound process, the rebound probability p_{reb} depends only on the ratio of the impact velocity v_{imp} to $\sqrt{gd}$. Following the numerical simulations by Werner (1988) and Anderson & Haff (1988, 1991), we will use the expression:

$$p_{\mathrm{reb}} = p_{\infty}\left[1 - \exp\left(-\frac{v_{\mathrm{imp}}}{a\sqrt{gd}}\right)\right]. \qquad (2.3)$$

The typical velocity $a\sqrt{gd}$ below which p_{reb} becomes very low can be interpreted as the velocity necessary to escape from the potential trapping at the sand bed surface (Quartier *et al.* 2000). We assume that the ejection speed is deterministic both in modulus

$$v_{\mathrm{eje}} = \gamma a\sqrt{gd} \qquad (2.4)$$

and in angle θ_{eje}. Again, this is the average behaviour observed numerically (Werner 1988; Anderson & Haff 1988, 1991) and experimentally (McEwan *et al.* 1992; Rioual *et al.* 2000). When the impact speed increases, it is not the ejection velocity that increases, but the number of ejecta. The results by Werner (1988), Anderson & Haff (1988, 1991) and McEwan *et al.* (1992) and Rioual *et al.* (2000) are consistent with the assumption that a constant fraction of the impact momentum is transferred to the ejecta. This means that the number of reptons produced by an impacting salton increases linearly with the impact speed:

$$N_{\mathrm{eje}} = \frac{v_{\mathrm{imp}}}{a\sqrt{gd}} - 1. \qquad (2.5)$$

Note that the critical velocity is chosen to ensure that reptons do not eject other grains. The choice of the same rescaled velocity a in the expressions of p_{reb}, v_{eje} and N_{eje} is for simplicity.

These average laws governing rebound and ejection should be regarded as reasonable first approximations. For instance, Ungar & Haff (1987) have assumed that a constant fraction of the kinetic energy is transferred to the ejecta so that (2.5) is replaced by $N_{\mathrm{eje}} \propto v_{\mathrm{imp}}^2/gd$. The existing measurements are not sufficiently precise to discriminate this possibility from the previous one. We choose here to remain close to the splash function obtained by Werner (1988) for the sake of comparison.

2.2. *The discrete states*

Let us assume for a short while that the velocity profile is known and let us follow the history of a typical grain. Its life starts when it is ejected – with a velocity v_{eje} and an angle θ_{eje} – by a salton. It makes a first flight, is accelerated by the wind and makes a first collision with the soil. It ejects a few other grains – more precisely N_{eje} – but there is a large probability that it will remain trapped. If it survives, part of its momentum is dissipated in the shock, but it is again accelerated during its second flight. Again it splashes reptons, but has a non-vanishing probability of being absorbed by the sand bed. Since the rebound probability is smaller than p_∞, the grain has a probability of surviving to n collisions which is bounded by $p_\infty{}^n$ and which thus decreases at least exponentially with n. In the saturated regime, a grain that remains trapped during one rebound or another is statistically replaced by an ejected grain; but contrary to the assumption of the one-species model, the velocities of the trapped and the ejected grains are different. The new grains always start with the ejection velocity v_{eje} and then follow the sequence flight/collision previously described.

In the saturated regime, all the grains follow exactly the same series of flights, starting from the ejection conditions. The only difference between the individual stories of the grains is the number of collisions before being trapped by the soil. In other words, the grain trajectory is deterministic, but it has a probability at each collision with the sand bed to keep going on or to stop. This is the picture following one single grain in time. If we now consider all the grains at a given time, they can be in a discrete number of states which correspond to the successive generations of grains and labelled by the collision number n. Each of these states is characterized by the trajectory after the nth rebound together with the fluxes of particles vertically ϕ_n and horizontally $q_n = \phi_n L_n$. The grains labelled $n+1$ result from the rebound of the grains labelled n and are thus characterized by:

$$\left.\begin{aligned}
\phi_{n+1} &= \phi_n\, p_{\text{reb}}\left(v_{\text{imp}}^n\right), \\
v_{\text{reb}}^{n+1} &= \gamma\, v_{\text{imp}}^n.
\end{aligned}\right\} \tag{2.6}$$

All the transported grains eject other grains when they collide with the sand bed. These ejecta are the grains labelled 0. At equilibrium, the flux of grains ejected ϕ_0 is equal to the sum of all the ejection fluxes due to all the generations of grains:

$$\left.\begin{aligned}
\phi_0 &= \sum_{n=1}^{+\infty} \phi_n N_{\text{eje}}\left(v_{\text{imp}}^n\right), \\
v_{\text{reb}}^0 &= v_{\text{eje}} = a\sqrt{gd}.
\end{aligned}\right\} \tag{2.7}$$

It is worth noting that the contribution of tractation to the flux ϕ_0 is neglected.

The trajectories of the grains depend on the wind velocity profile $u(z)$. When the wind blows over a rough solid plate made of glued grains, this profile is usually found to increase logarithmically with height z:

$$u_0(z) = \frac{u_*}{\kappa}\ln\frac{z}{z_0}, \tag{2.8}$$

If the grains are larger than the viscous sublayer ($d > \nu/u_*$, where ν is the air viscosity), the roughness z_0 scales on the grain size ($z_0 = rd$). The logarithmic profile can be simply understood in the context of turbulent boundary-layer theory. The Prandtl

Variable	Parameter	Value
ρ_{sand}/ρ_{air}	Density contrast	2208
C_D	Drag coefficient	1
γ	Restitution coefficient of grain bed collision	0.5
p_∞	Rebound probability for a large velocity grain	0.95
θ_{reb}	Rebound angle	45°
a	Escape velocity rescaled by $\sqrt{gd}$	10
θ_{eje}	Ejection angle	45°
r	Aerodynamic roughness rescaled by the grain diameter d	1/30
κ	Von Kármán constant	0.4

TABLE 1. Values of the quantities used in the model.

turbulent closure relates the air shear stress τ_{air} to the velocity gradient $\partial_z u$ by:

$$\tau_{air} = \rho_{air} \left(\kappa \frac{\partial u}{\partial \ln z} \right)^2, \tag{2.9}$$

where $\kappa \simeq 0.4$ is the von Kármán constant. Finally, the wind is modified by all the transported grains according to the momentum balance:

$$\tau_{air} = \rho_{air} \left(\kappa \frac{\partial u}{\partial \ln z} \right)^2 = \rho_{air} u_*^2 - \sum_{n=0}^{+\infty} \phi_n(v_\downarrow^n - v_\uparrow^n). \tag{2.10}$$

Table 1 shows the values of the different parameters used in the numerical resolution of the model. They correspond to standard values found in the literature. The numerical procedure to find the equilibrium state is simple and is composed by two interwoven steps.

(i) For a fixed value of ϕ_0, we solve the mechanical equilibrium (2.10) to find the velocity profile $u(z)$. For this, we start from the undisturbed velocity profile (2.8) and compute the grain trajectory starting from the ejection condition. This allows us to compute $v_\downarrow^n - v_\uparrow^n$ and the flux ϕ_n of grains from the nth generation. From this, a refined estimate of the wind velocity profile can be deduced using (2.10). These two substeps are repeated iteratively until a steady solution is reached.

(ii) The problem is then to find the value of ϕ_0 for which this steady solution also verifies the balance (2.7) between the number of ejecta and the number of grains trapped. This is achieved by a common solving method (bracketing and bisection).

2.3. Results

In the following, we will discuss the properties of the saturated state. We will present the results for two shear velocities, one just above the threshold, $u_* = 5\sqrt{gd}$, and the other far above, $u_* = 20\sqrt{gd}$. The path of a grain which would, casually, remain 'alive' in its first twenty bounces is shown on figure 2. Apart from around the starting point, the trajectory is apparently very similar to that of a grain in an undisturbed wind (Owen 1964; Sørensen 1991; Nalpanis *et al.* 1993). In particular, it eventually reaches a permanent state which depends on the wind strength: the height H_∞ and length L_∞ of the limit trajectory are much larger for $u_* = 20\sqrt{gd}$ than for $u_* = 5\sqrt{gd}$.

The lengths and heights of the successive jumps are shown in figure 3 as a function of the collision number n. It shows a striking feature: before being accelerated by the wind, the grain in fact makes a dozen small-altitude flights. This low-energy state is almost independent of the wind strength: both for $u_* = 5\sqrt{gd}$ and $u_* = 20\sqrt{gd}$, the hop height H_n is between 5 and 10 grain diameters and the hop length L_n between 50 and
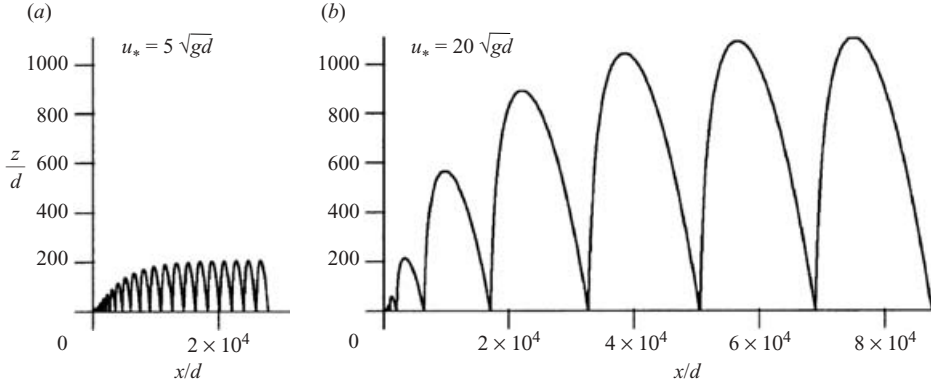
FIGURE 2. Trajectory of a grain for two wind speeds ((a) $u_* = 5\sqrt{gd}$ and (b) $u_* = 20\sqrt{gd}$), as predicted by the n-generations model. The grain is initially a repton ejected from the bed by another grain and is progressively accelerated by the wind. By assumption, the grain ejects N_{eje} other grains when it collides with the soil but has also a non-vanishing probability $1 - p_{reb}$ of remaining trapped.
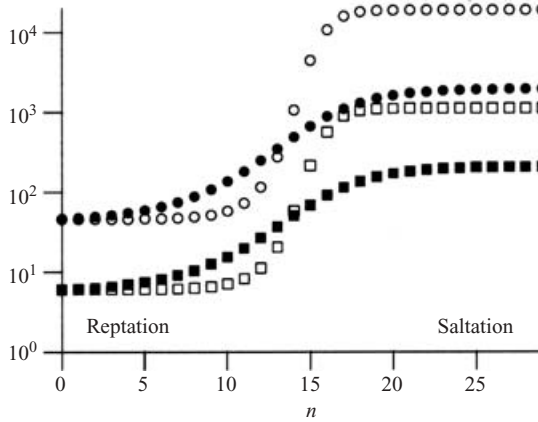

FIGURE 3. Lengths L (circle) and heights H (square) of the grain trajectories as a function of the number n of rebounds since their first ejection. The points are computed for $u_* = 5\sqrt{gd}$ (black symbol) and $u_* = 20\sqrt{gd}$ (open symbol) according to the n-generations model. Note the logarithmic scale on the vertical axis. One grain is first ejected by another grain ($n = 0$). It then makes between $n = 10$ and $n = 15$ small jumps of height $H \simeq 5 - 10\,d$ and of length $L \simeq 50 - 100\,d$ (reptation). It is then accelerated by the wind as it would be if it were isolated and reaches a high-energy permanent state (saltation).

$100\,d$. This is precisely the characteristic of reptation. From $n = 12$ to $n = 17$, the grain enters the saltation layer and is accelerated. At $n \simeq 18$, it reaches a permanent state which depends on the shear velocity u_* (figures 2 and 3). In conclusion, there are two well-defined species of grain where an infinite though discrete number of states was expected.

Figure 4 shows the contribution of the generation n to the sand transport. Again, three regions can be distinguished: reptons from $n = 0$ to $n = 10 - 12$, saltons from $n = 16 - 20$ to infinity and the transition between the two which corresponds to the phase of acceleration of the grains. In both reptation and saltation regimes, the flux $q_n = \phi_n L_n$ decreases exponentially with n. This is not due to the hop length L_n which
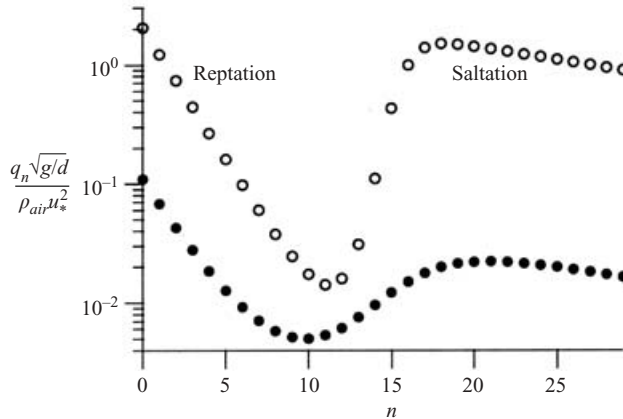
FIGURE 4. Flux q_n of grains of generation n, rescaled by $\rho_{air} u_*^2 \sqrt{d/g}$. The black circles are computed for $u_* = 5\sqrt{gd}$ and the open circles for $u_* = 20\sqrt{gd}$, in the saturated regime.

depends only weakly on n (figure 3), but to the absorption of grains during collisions. Let us detail the case of saltation. Denoting by v_{imp}^{∞} the limit impact velocity, the grain has, even in this large-energy state, a probability $p_{reb}^{\infty} = p_{reb}(v_{imp}^{\infty})$ smaller than 1 of rebounding. As a consequence, the horizontal flux decreases for large n as:

$$\phi_n \propto (p_{reb}^{\infty})^n. \tag{2.11}$$

For $u_* = 20\sqrt{gd}$, this approximation is valid for $n > 20$ (figure 3). This is used in practice to close the system of equations at $n = 50$ and to integrate it numerically. Thus, the slope of $\ln q_n$ function of n is directly related to the probability of rebound p_{reb}. Since reptons have a larger probability of remaining trapped (equation (2.3)), the flux q_n decreases much faster with n in the reptation than in the saltation regime. During the transition from reptation to saltation, the flux q_n increases because, this time, L_n increases (figure 3). It is worth noting that the vertical flux ϕ_n can only decrease with n because some of the grains are trapped during the collisions (equation (2.6)). However, this does not preclude the increase with n of the horizontal flux q_n, which also depends on the grain hop length.

Figure 5(a) shows the wind velocity profile $u(z)$ modified by the sand transport. Just above the threshold, for $u_* = 5\sqrt{gd}$, $u(z)$ is almost undisturbed. We will use this property to derive the expression of the threshold velocity in §3.2. For $u_* = 20\sqrt{gd}$, there is a negative feedback of the sand transport on the wind velocity profile as it is far above the threshold. Above the saltation layer ($z > H_{sal}$), $u(z)$ is as expected a logarithmic profile but with an increased roughness z_0. In practice, we measured z_0 just at the saltation height:

$$z_0 = H_{sal} \exp\left(-\frac{\kappa u(H_{sal})}{u_*}\right).$$

Inside the saltation layer ($H_{rep} < z < H_{sal}$), the wind velocity is almost undisturbed (it is in fact slightly reduced), whereas it is strongly reduced inside the reptation layer ($z < H_{rep}$). It can be remarked that the profiles obtained for the two velocities are closed to each other inside the reptation layer. Thus, $u(z)$ remains almost equal to the profile at threshold,

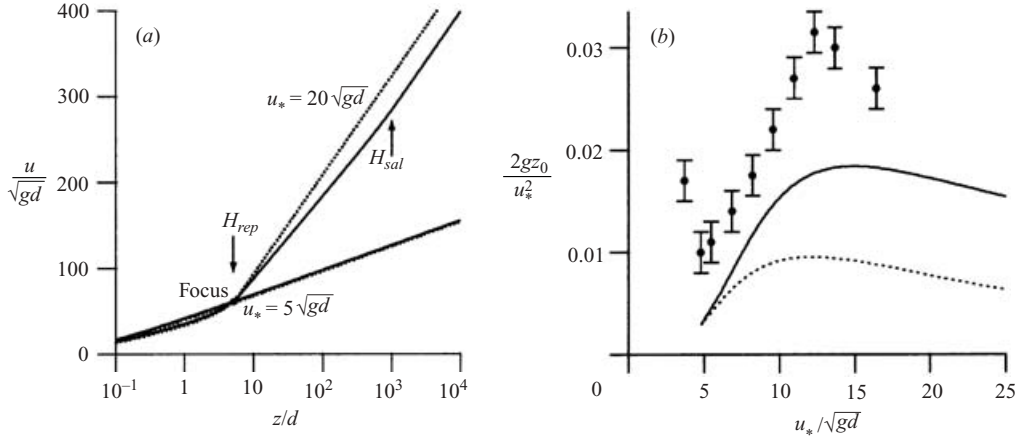$$u(z) \simeq \frac{u_{th}}{\kappa} \ln \frac{z}{rd} \qquad (z < H_{rep}).$$

FIGURE 5. (a) Rescaled velocity profile $u(z)/\sqrt{gd}$ at saturation for $u_* = 5\sqrt{gd}$ and $u_* = 20\sqrt{gd}$ solving numerically the n-generations model equations (solid lines). The wind is strongly reduced in the reptation layer, but is practically unaffected in the saltation layer. The dotted line corresponds to the profile computed without the contribution of saltation ($n > n_{rs}$) to the sand-borne shear stress. The profiles obtained for different u_* cross each other in a small region of the figure called the focus. (b) Rescaled roughness $2gz_0/u_*^2$ as a function of the rescaled shear velocity $u_*/\sqrt{gd}$ measured by Rasmussen *et al.* 1996 for 544 µm grains (black circles) and predicted by the n generations model (solid line). The dotted line is the same quantity computed without the contribution of saltation ($n > n_{rs}$).

In the second approximation, the velocity profiles depart from this logarithmic approximation as the shear velocity increases, but they cross each other in a small region around $z = H_F$ and $u = U_F$ called the focus. This was observed experimentally by Bagnold (1941) and in the numerical model by Werner (1988). It is also predicted by the one-species model (Ungar & Haff 1987) and that for an excellent reason: during the first rebounds, the grain makes almost the same flight and this is precisely the requirement of the one-species model. As a conclusion, the reptation layer behaves as predicted by the one-species model (see §1).

In order to compute the contribution of reptation and saltation to the wind velocity reduction, we will use the minimum of the curve q_n/u_*^2 as the limit n_{rs} between the two species. The generations n from 0 to n_{rs} are reptons and above n_{rs} are saltons. For $u_* = 20$, we see in figure 4 that $n_{rs} = 11$. We have checked that any other reasonable criterion (for instance the inflection point of q_n) gives almost the same results. We have computed the wind profile that would have been obtained if only reptation was contributing to the sand-borne shear stress. In practice, we integrate the equation

$$\rho_{air}\left(\kappa\,\frac{\partial u}{\partial \ln z}\right)^2 = \rho_{air}u_*^2 - \sum_{n=0}^{n_{rs}}\phi_n(v_\downarrow^n - v_\uparrow^n), \qquad (2.12)$$

keeping the same values of ϕ_n, $v_\downarrow^n$ and $v_\uparrow^n$. This virtual velocity profile is shown by the dotted line in figure 5(a). The contribution of saltation is negligible inside the reptation layer. It has a slight effect on the velocity profile inside the saltation curtain. But this change of $u(z)$ by less than 15% results in an important increase of the aerodynamic roughness z_0. This is confirmed in figure 5(b) where z_0 is plotted as a function of the shear velocity u_*. In order to compare the result to the Owen (1964) model, z_0 is rescaled by the typical saltation layer height $u_*^2/2g$. It is compared to the value
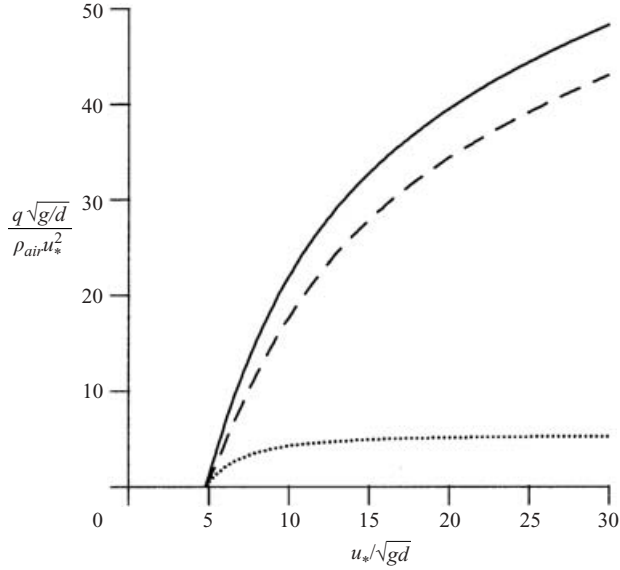
FIGURE 6. Saturated flux q rescaled by $\rho_{air} u_*^2 \sqrt{d/g}$ as a function of the rescaled shear velocity $u_*/\sqrt{gd}$, computed from the n-generations model. The total flux (solid line) is decomposed into the contribution of reptons (dotted line) and that of saltons (dashed line). The ratio between the flux of saltons and the flux of reptons varies from 1.5 to 9 in the range of shear velocities shown.

it would have if the contribution of saltation to the sand-borne shear stress was negligible (equation (2.12)). There is a factor of two between the two.

As a conclusion, looking at the velocity profiles, the wind reduction is almost due to reptation only and limited to the reptation layer. The apparent roughness z_0 is a complex quantity that is also very sensitive to the slight wind reduction in the saltation layer. The shape of the curve andthe order of magnitude of the roughness are similar to that measured by Rasmussen *et al.* 1996 (black circles with error bars). In all cases, the aerodynamic roughness is much smaller than the saltation height H_{sal}. In the Appendix, we compare in a systematic way the measurements of z_0 by Rasmussen *et al.* 1996 to the prediction obtained assuming the existence of a focus. We show that it correctly gives the dependence of z_0 with u_*, but that an extra-dependence on the grain diameter d is found, ascribed to a Reynolds-number effect.

These results show that the scenario of sand transport saturation is different from that assumed in the one-species model. The reptons are mostly ejected by the saltons, but, in turn, the saltons come from the acceleration of reptons by the wind. From the point of view of saltons, the saturation occurs when the number of reptons promoted to saltation has become so small that it just balances the number of saltons that remain trapped in the collisions. The number of reptons increases with the number of saltons because they are splashed by the latter. As a consequence, the wind speed in the reptation layer decreases and the reptons remain more and more in the reptation state. From the point of view of reptons, the saturation happens when the wind speed in the reptation layer is so close to its threshold value that most of the reptons are absorbed by the sand bed and only a few of them are promoted to saltation.

Figure 6 shows the saturated flux q, computed numerically from the n-generations model. q vanishes below a threshold shear velocity $u_{th} \simeq 4.9\sqrt{gd}$ and above the

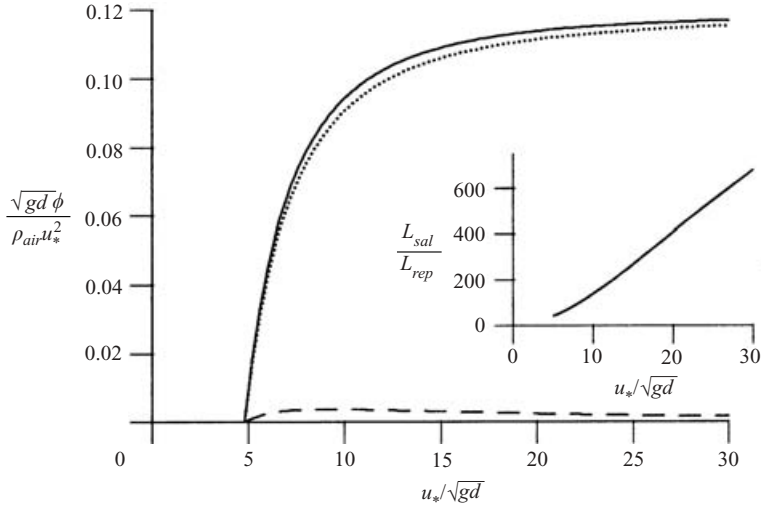FIGURE 7. Vertical flux ϕ rescaled by $\rho_{air}u_*^2/\sqrt{gd}$ as a function of the rescaled shear velocity $u_*/\sqrt{gd}$, computed from the *n*-generations model. The total flux (solid line) is decomposed into the contribution of reptons (dotted line) and that of saltons (dashed line). Contrary to the horizontal flux q (figure 6), ϕ asymptotically scales with u_*^2 and the contribution of saltons to this flux tends to 0. Inset: ratio of the saltons hop length L_{sal} to that of the reptons L_{rep} as a function of u_*.

threshold it increases faster than u_*^2. The flux is described well by the empirical scaling law proposed by Werner (1990):

$$q \propto \left(u_*^2 - u_{th}^2\right)^{\delta}$$

and we find the same exponent $\delta \simeq 1.2$. Globally, there is a strong similarity between the results (velocity profiles, velocity–flux relationship) of the *n*-generations model and that proposed by Werner (1990). This means that the randomness introduced in the rebound/ejection laws is inessential. We can thus keep going on safely in our quest for the relevant dynamical mechanisms.

Figure 6 shows the reptation flux (dotted line) and the saltation flux (dashed line) together with the total flux. We can see that the reptation flux scales as u_*^2 for large u_*, just like the Ungar & Haff (1987) model. On the other hand, the saltation flux increases faster than u_*^2 and gives the dominant contribution to the total flux. We have plotted on figure 7 the vertical flux ϕ, also decomposed into reptons and saltons. Contrarily to q, ϕ is dominated by the reptons and thus scales asymptotically as u_*^2. This means that most of the grains leaving the soil are reptons but that the major part of transport is still due to saltons. As can be seen from the inset of figure 7, this is due to the large saltation length L_{sal} compared to the hop length of reptons L_{rep}. Saltons contribute to the sand transport (to q) because of their velocity and reptons because of their number.

As a conclusion, the *n*-generations model allows us to solve the problems arising in the one-species models. It gives a self-consistent and stable solution in which saltons and reptons play specific roles. Our aim is now to simplify the description and to reintroduce space and time variations in order to investigate the saturation transient.
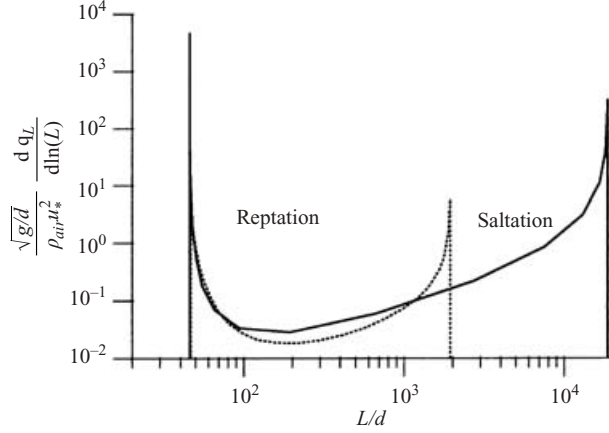
FIGURE 8. Flux density $dq_L/d\ln(L)$ as a function of the hop length L for $u_* = 5\sqrt{gd}$ (dotted line) and $u_* = 20\sqrt{gd}$ (solid line) according to the n-generations model. The two peaks indicate two well-defined species corresponding to reptons and saltons. Note the log–log scale.

3. The two-species model

3.1. *From n to 2 species*

In the n-generations model, two types of trajectory corresponding to saltation and reptation appear in the solution; they were not forced by the assumptions of the model. To clarify the status of these two modes of transport, we define q_L as the part of the flux q due to grains whose hop length is smaller than L. Figure 8 shows the flux density $dq_L/d\ln(L)$ which can be interpreted as a distribution of hop lengths weighted by their contributions to the flux. It exhibits two strong peaks separated by a range of L in which the sand transport is low. So, reptation and saltation are – in the model – not the extreme states of a continuous distribution but two distinct species of grain. Of course, the peaks would be flattened if a realistic splash function were used. Still, we expect them to be visible in experimental measurements. It is worth insisting on the fact that q_L is the correct quantity to be measured. It is not equivalent to the vertical profile of concentration, which mixes the different trajectories. It is not equivalent to the distributions of L weighted by the density of grains or weighted by ϕ, which essentially has one single peak corresponding to reptation.

We will now simplify the description of the problem, assuming that each of the two species corresponds to a well-defined and unique trajectory. The reptons have a shorter life-time than the saltons because they have a much larger probability $p_{rep} > p_{sal}$ of remaining trapped when they collide with the soil. Besides, they are continuously ejected from the sand bed by the impacting saltons, each salton producing N_{eje} reptons per collision. The probabilities p_{rep} and p_{sal} are assumed to be constant. Note that p_{rep} is $1 - p_{reb}(v_{imp}^{rep})$. The characteristics of reptation (flight time T_{rep} and hop length T_{rep}) are assumed to be constant. The characteristics of saltation (flight time T_{sal}, hop length L_{sal} and number of ejecta N_{eje}) are assumed to be functions of u_* only.

Introducing the vertical fluxes of saltons and reptons ϕ_{sal} and ϕ_{rep}, the conservation of matter for the two species reads:

$$\left.\begin{aligned} T_{rep}\partial_t\phi_{rep} + L_{rep}\partial_x\phi_{rep} &= -p_{rep}\phi_{rep} - \varphi + N_{eje}\phi_{sal} \\ T_{sal}\partial_t\phi_{sal} + L_{sal}\partial_x\phi_{sal} &= -p_{sal}\phi_{sal} + \varphi \end{aligned}\right\} \tag{3.1}$$
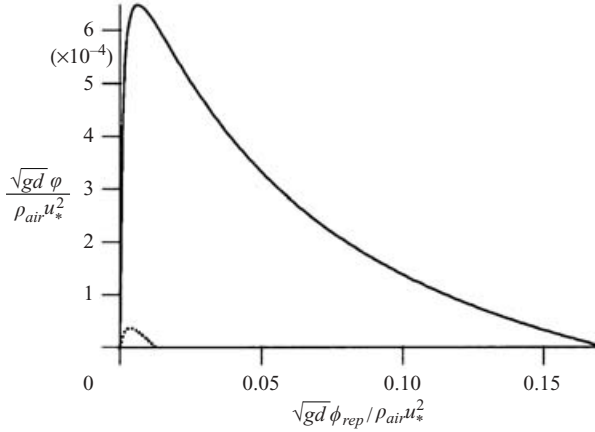
FIGURE 9. Flux φ of reptons promoted to saltation for $u_* = 5\sqrt{gd}$ (dotted line), and $u_* = 20\sqrt{gd}$ (solid line) according to the n-generations model.

Again, we have completely neglected the production of reptons by tractation. This could be taken into account by adding a third conservation equation for tractons similar to that used to describe avalanches (Douady, Andreotti & Daerr 1999). We do not need it to understand the mechanisms of saturation, but it could be important to describe the formation of sand ripples.

The flux φ is the mass of reptons promoted to saltation per unit time and unit surface. It is the key quantity of these equations as it encodes the negative feedback of sand transport on the air velocity. The wind velocity reduction takes place mostly inside the reptation layer. φ should thus essentially depend on the reptation flux ϕ_{rep} and on the shear velocity u_*. Again, we can use the n-generations model to measure it. We first choose a criterion to separate reptation from saltation: we consider that a repton has been promoted to saltation when its hop height becomes larger than a threshold H_{rs} (in practice, we have taken $H_{rs} = 15d$, see figure 3). This occurs between the rebound number n_{rs} and $n_{rs} + 1$: $H_{n_{rs}} < H_{rs} < H_{n_{rs}+1}$. We perform a linear interpolation between two simple cases: if $H_{n_{rs}} = H_{rs}$, φ is simply the flux $\phi_{n_{rs}+1}$ of grains belonging to the species $n_{rs} + 1$; if $H_{n_{rs}+1} = H_{rs}$, φ is simply the flux $\phi_{n_{rs}+2}$. In between, we obtained:

$$\varphi \simeq \phi_{n_{rs}+1} + \left(\phi_{n_{rs}+2} - \phi_{n_{rs}+1}\right) \frac{H_{rs} - H_{n_{rs}}}{H_{n_{rs}+1} - H_{n_{rs}}}.$$

Figure 9 shows the relation between φ and ϕ_{rep} for $u_* = 5\sqrt{gd}$ and $u_* = 20\sqrt{gd}$. To obtain this curve, we varied ϕ_0 systematically for a given u_*, solved the mechanical equilibrium (2.10) and measured φ and ϕ_{rep}. This simply means that φ is measured when the wind is at equilibrium with the sand transport, but when the flux is not saturated.

If there is no sand transport ($\phi_{rep} = 0$), no grain is promoted to saltation ($\varphi = 0$). At very low reptation flux, it induces almost no reduction of the wind speed: all the reptons are quickly promoted to saltation. This corresponds in figure 9 to the slope of order 1 near the origin. When the reptation flux becomes sufficiently important to reduce significantly the wind velocity inside the reptation layer, the flux of reptons promoted to saltation starts decreasing with ϕ_{rep} and vanishes for a value of ϕ_{rep} scaling as $\rho_{air}(u_*^2 - u_{th}^2)/\sqrt{gd}$.
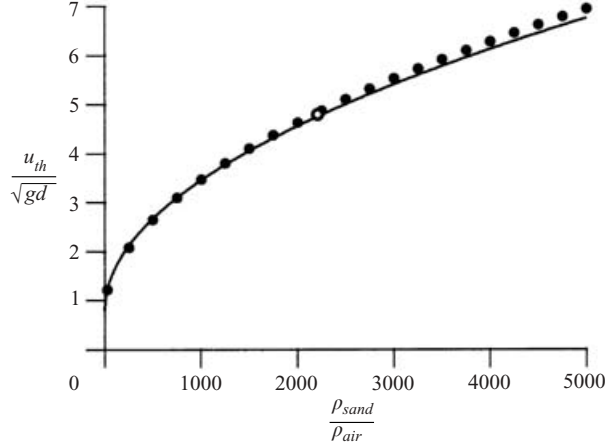
FIGURE 10. Threshold velocity as a function of the particle to fluid density ratio ρ_{sand}/ρ_{air} according to the n-generations model (black circle). The open circle corresponds to the reference value of the quartz to air density ratio: $\rho_{sand}/\rho_{air} = 2208$. The solid line is the analytical approximation given in the text.

3.2. Threshold velocity

u_{th} is the shear velocity for which the impact velocity v_{imp}^{rep} of a repton in the undisturbed boundary layer is equal to the critical value $a\sqrt{gd}$. In that case, the loss of momentum in the collisions is balanced by the fluid drag integrated along the trajectory. In a first approximation, this gives:

$$\frac{dv}{dt} \simeq \frac{v_{imp}^{rep}(1 - \gamma\cos\theta_{rep})}{T_{rep}} \simeq \frac{1 - \gamma\cos\theta_{rep}}{\sin\theta_{rep}} g.$$

The typical wind velocity to which the repton is submitted is of the order of:

$$u \simeq \frac{u_{th}}{\kappa}\ln\frac{H_{rep}}{2rd} \simeq \frac{u_{th}}{\kappa}\ln\frac{(a\gamma\sin\theta_{rep})^2}{2r}.$$

Assuming that the drag is turbulent (equation (2.1)), we easily obtain an approximation of the threshold velocity as:

$$\frac{u_{th}}{\sqrt{gd}} \simeq \frac{\kappa}{\ln\dfrac{(a\gamma\sin\theta_{rep})^2}{2r}}\left(a + \sqrt{\frac{4(1 - \gamma\cos\theta_{rep})}{3C_D\sin\theta_{rep}}\frac{\rho_{sand}}{\rho_{air}}}\right). \tag{3.2}$$

This prediction is plotted as a function of the density ratio ρ_{sand}/ρ_{air} in figure 10 (solid line). The black circles correspond to the same quantity computed numerically according to the n-generations model. The agreement between the two validates our approximations. The measurements reported by Iversen & Rasmussen (1994, 1999) are consistent with the scaling predicted (see the Appendix and in particular figure 12):

$$u_{th} \simeq 4.7\sqrt{gd}.$$

This is exactly the value predicted by (3.2) for $C_D = 1$, $\theta_{rep} = 45°$, $\gamma = 0.5$ and $a = 10$. Of course, we cannot fix four independent parameters with one measurement, but at

least they are consistent with the measurements. Note that u_{th} is linearly related to a, which is the most difficult parameter to estimate from prior considerations.

3.3. *Saturated state*

After sufficient space and time, the sand transport saturates. The fluxes are steady and homogeneous so that the conservation of matter (3.1) simplifies in:

$$\left.\begin{array}{l} \varphi = N_{\text{eje}}\phi_{\text{sal}} - p_{\text{rep}}\phi_{\text{rep}}, \\ \varphi = p_{\text{sal}}\phi_{\text{sal}}. \end{array}\right\} \tag{3.3}$$

On one hand, the flux of reptons promoted to saltation is equal to the difference between the production and the absorption of reptons; on the other hand, this flux balances the absorption of saltons. This fixes the ratio of the saltation to reptation fluxes:

$$\phi_{\text{sal}} = \frac{p_{\text{rep}}}{N_{\text{eje}} - p_{\text{sal}}}\phi_{\text{rep}}. \tag{3.4}$$

The saltons have also a small but non-vanishing probability of remaining trapped when they collide with the sand bed. To balance the small loss in saltons, there should be a small creation of saltons from reptons:

$$\frac{\varphi}{\phi_{\text{rep}}} = \frac{p_{\text{sal}}p_{\text{rep}}}{N_{\text{eje}} - p_{\text{sal}}} \ll 1. \tag{3.5}$$

This condition can be solved explicitly from the relation between φ and ϕ_{rep}. It expresses the requirement that the wind inside the reptation layer should have so decreased that the impact velocity $v_{\text{imp}}^{\text{rep}}$ of the reptons becomes almost equal to its threshold value $a\sqrt{gd}$. This is precisely the condition of equilibrium prescribed in the Ungar & Haff (1987) model. So, at equilibrium, the reptation flux scales as:

$$\phi_{\text{rep}} \propto \rho_{\text{air}}\left(u_*^2 - u_{th}^2\right)\frac{T_{\text{rep}}}{L_{\text{rep}}}. \tag{3.6}$$

We finally obtain the expressions of the reptation and saltation fluxes:

$$\left.\begin{array}{l} q_{\text{rep}} = \alpha\rho_{\text{air}}\left(u_*^2 - u_{th}^2\right)T_{\text{rep}}, \\ q_{\text{sal}} = \dfrac{p_{\text{rep}}L_{\text{sal}}}{(N_{\text{eje}} - p_{\text{sal}})L_{\text{rep}}}q_{\text{rep}}. \end{array}\right\} \tag{3.7}$$

This prediction of the saturated flux cannot be reduced to that of a one-species as the dynamical mechanisms are different. The total flux q is scaling asymptotically as $u_*^2 T_{\text{sal}}$ in Owen-like models and as $u_*^2 T_{\text{rep}}$ for Ungar & Haff (1987). We find here an asymptotic scaling as $u_*^2 L_{\text{sal}}/N_{\text{eje}}$. The complicated dependence of L_{sal} and N_{eje} on u_* is at the origin of the apparent scaling as $(u_*^2 - u_{th}^2)^{1.2}$ found both in Werner (1990) and in the n-generations model.

In the Appendix, we compare in a systematic way the flux measurements by Iverser & Rasmussen (1999) to (3.7). Again, it is difficult to extract information about the parameters of the model. A first simplification is to consider that T_{rep} is the lifetime of reptons so that:

$$p_{\text{rep}} = 1. \tag{3.8}$$

Since p_{sal} is much smaller than N_{eje}, (3.7) reduces to:

$$q_{\text{sal}} = \frac{L_{\text{sal}}}{N_{\text{eje}}L_{\text{rep}}}q_{\text{rep}}. \tag{3.9}$$

Then, the analysis of experimental data shows that the dependence of the flux with u_* is correctly described if (2.5) giving N_{eje} is changed for:

$$N_{\text{eje}} \simeq 0.3 \left(\frac{v_{\text{imp}}}{a\sqrt{gd}} \right)^2 . \qquad (3.10)$$

This precisely corresponds to the hypothesis made by Ungar & Haff (1987) that a constant fraction of the energy of an impacting salton is transmitted to the ejecta. α is found to be of order unity, but exhibits an extra-dependence on the grain diameter d, ascribed to a Reynolds-number effect.

3.4. *Transient: the saturation length*

We have shown in previous works (Andreotti *et al.* 2002*a, b*; Hersen, Douady & Andreotti 2002) that the only relevant lengthscale in the dune problem is the spatial lag before saturation. This saturation length λ_{sat} has been measured directly by Bagnold (1941) and has been estimated through the size of proto-dunes by Andreotti *et al.* (2002*b*) and through the cut-off that appears in the relationship between the velocity of barchan dunes and their width by Hersen *et al.* 2004: it is between 3 m and 7 m. Apart from in the phenomenological model built by Sauermann *et al.* 2001 (see also Andreotti *et al.* 2002*a*), this length has not received any theoretical prediction so far. The problem about this length is essentially to explain why it does not scale on the saltation length (Bagnold 1941) and why it is so large, compared to the length λ_{drag} needed to accelerate static grains to the wind velocity:

$$\lambda_{\text{drag}} = \frac{\rho_{\text{sand}}}{\rho_{\text{air}}} d. \qquad (3.11)$$

For typical sand grains of 180 μm, $\lambda_{\text{drag}} = 40$ cm.

We have computed numerically the solution of the two-species model using the characteristics of reptation and saltation determined from the *n*-generations model. N_{eje} is modelled according to (3.10) and the two probabilities of absorption are $p_{\text{rep}} = 1$ and $p_{\text{sal}} = 0.05$. We consider the transition between the solid ground and a flat sand bed: at $x = 0$, we put a very low sand transport and compute the steady but inhomogeneous solutions of (3.7). The result is shown in figure 11(*a*) for two different wind velocities. Just above the threshold ($u_* = 5\sqrt{gd}$), we observe a long exponential increase of fluxes over approximately $20\lambda_{\text{drag}}$ that corresponds to the phase where a grain ejected is almost immediately promoted to saltation and ejects N_{eje} other grains. Then, the negative feedback of reptation on the wind becomes important and the fluxes relax exponentially towards their saturated values. At high velocity ($u_* = 20\sqrt{gd}$ in figure 11*a*), the first phase is almost invisible and the whole dynamics can be described by a simple relaxation equation:

$$\partial_x q = \frac{q_{\text{sat}} - q}{\lambda_{\text{sat}}}. \qquad (3.12)$$

To find analytically the different lengthscales involved in this transient, we perform the stability analysis around the two equilibrium solutions: null flux and saturated flux. We denote by $\tilde{\phi}_{\text{rep}}$ (resp. $\tilde{\phi}_{\text{sal}}$) the difference between ϕ_{rep} (resp. ϕ_{sal}) and its value at equilibrium. The only nonlinearity in (3.1) comes from the flux φ of reptons promoted to saltation. We introduce φ', the derivative of φ with respect to ϕ_{rep} at equilibrium. For a vanishing transport, $\varphi' = \varphi'_e$ is positive and of order unity; at saturation, $\varphi' = \varphi'_s$ is negative and of the order of -10^{-3}. Assuming a steady flux, the
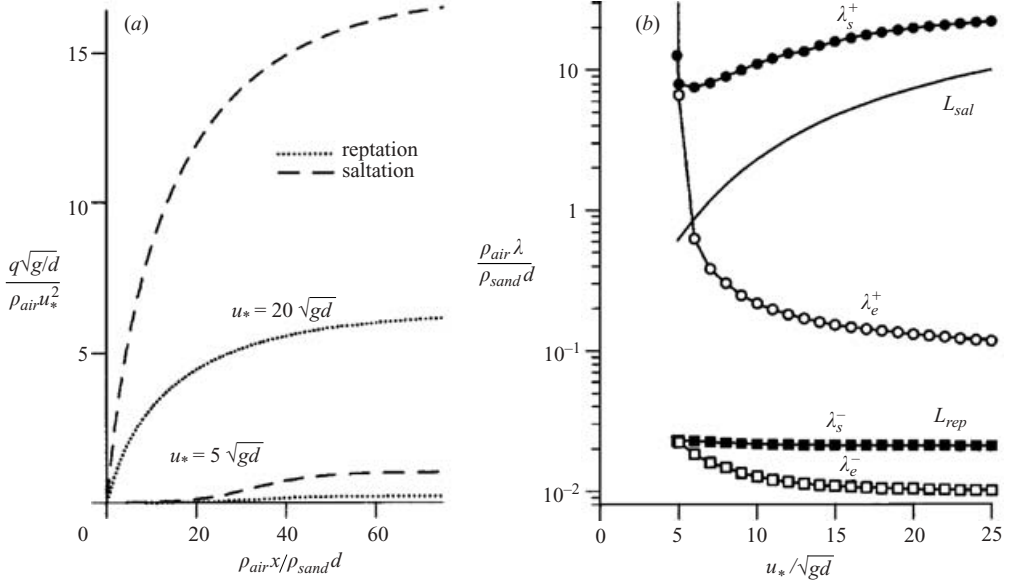
FIGURE 11. Transient of saturation. (*a*) Saltation and reptation fluxes as functions of the horizontal coordinate rescaled by λ_{drag} for $u_* = 5\sqrt{gd}$ and $u_* = 20\sqrt{gd}$ according to the two-species model. (*b*) The linear analysis for a vanishing transport gives two modes, one increasing exponentially over a length λ_e^+ and the other decaying over λ_e^-. The linear analysis, this time around the saturation gives two decaying modes, one over a length λ_s^- almost equal to the reptation length and the other over a very long length λ_s^+ which gives the most significant contribution to the saturation length.

linearization of (3.1) results in:

$$L_{\mathrm{rep}}\partial_x\tilde{\phi}_{\mathrm{rep}} = -(p_{\mathrm{rep}} + \varphi')\tilde{\phi}_{\mathrm{rep}} + N_{\mathrm{eje}}\tilde{\phi}_{\mathrm{sal}}, \left.\begin{array}{c}\\\\\end{array}\right\} \tag{3.13}$$
$$L_{\mathrm{sal}}\partial_x\tilde{\phi}_{\mathrm{sal}} = \varphi'\tilde{\phi}_{\mathrm{rep}} - p_{\mathrm{sal}}\tilde{\phi}_{\mathrm{sal}}.$$

This equation set admits two solutions of the form $\exp(-x/\lambda)$, where λ verifies:

$$[p_{\mathrm{sal}}(p_{\mathrm{rep}} + \varphi') - N_{\mathrm{eje}}\varphi']\lambda^2 - [p_{\mathrm{sal}}L_{\mathrm{rep}} + (p_{\mathrm{rep}} + \varphi')L_{\mathrm{sal}}]\lambda + L_{\mathrm{rep}}L_{\mathrm{sal}} = 0. \tag{3.14}$$

Figure 11 shows the solutions of (3.14) as a function of the wind speed. For vanishing flux, one the two modes decays over a short length λ_e^- and the other amplifies over a length λ_e^+. Note that the solution in the latter case is $\lambda = -\lambda_e^+$. Around saturation, there are two decaying solutions, one with a very short length λ_s^- almost equal to the reptation length and the other with a very long length λ_s^+. Looking at the different orders of magnitude, the terms of (3.14) involving the probability p_{sal} of saltons remaining trapped during a rebound are negligible. Equation (3.14) can be reasonably approximated by $N_{\mathrm{eje}}\varphi'\lambda^2 + (p_{\mathrm{rep}} + \varphi')L_{\mathrm{sal}}\lambda - L_{\mathrm{rep}}L_{\mathrm{sal}} = 0$. The dimensionless quantity $N_{\mathrm{eje}}\varphi'L_{\mathrm{rep}}/((p_{\mathrm{rep}} + \varphi')L_{\mathrm{sal}})$ turns out to be small. Then, a first-order approximation of the solutions is:

$$\lambda^- \simeq L_{\mathrm{rep}}, \qquad \lambda^+ \simeq \frac{(p_{\mathrm{rep}} + \varphi')\, L_{\mathrm{sal}}}{-\varphi'\, N_{\mathrm{eje}}}.$$

This allows us to give an interpretation of the two modes. As reptons have a low probability of surviving to many rebounds, a local equilibrium between production and absorption of reptons is quickly reached. This means that typically after one

reptation length (λ^-), the ratio of the reptation to the saltation flux is fixed to:

$$\frac{\phi_{\text{rep}}}{\phi_{\text{sal}}} \simeq \frac{N_{\text{eje}}}{p_{\text{rep}}}. \tag{3.15}$$

The saturation transient is due to the slow promotion of reptons to saltation. There is a scale separation between the lengths after which the reptation flux is in equilibrium with the saltation flux and the saturation length:

$$\lambda_{\text{sat}} \simeq \lambda_s^+ \simeq \frac{p_{\text{rep}} L_{\text{sal}}}{-\varphi_s' N_{\text{eje}}}. \tag{3.16}$$

To conclude, let us turn to the variation of the saturation length with the shear velocity u_* (figure 11). λ_s^+ gently increases from $7.5\lambda_{\text{drag}} \simeq 3\,\text{m}$ to $20\lambda_{\text{drag}} \simeq 8\,\text{m}$. The order of magnitude is thus comparable to field observations. As the saturation length is a relaxation length, it should diverge at the threshold as in any other bifurcation. Figure 11 shows that this is indeed the case, but it can be observed that this divergence starts very close to the threshold.

4. Conclusion

In this paper we have discussed the dynamical mechanisms governing the saturation of aeolian sand transport. Our starting point was to show that all the previous models except one were inconsistent: if the wind speed is assumed to decrease to some threshold value inside the saltation layer then the grains should also have trajectories independent of the wind strength. The only self-consistent model based on the assumption that the trajectory of one particle is identical to that of any other is that by Ungar & Haff (1987). We have shown that it is not realistic since it predicts that all the sand transport takes place in the reptation layer, at few millimetres from the sand bed. Furthermore, it corresponds to an unstable solution.

We have proposed an alternative scenario for the saturation of sand transport, in which there is coexistence of high energy grains (saltons) and grains making small jumps of the order of a few grain diameters (reptons). The reptons have a small velocity and thus a very short life-time. However, there is a continuous ejection of reptons from the sand bed owing to the impacting saltons. The saltons, on the contrary, have a small probability of remaining trapped when they collide with the soil. This small loss is balanced by the promotion of a small fraction of the reptons to saltation. The saturation of the sand transport is due to the feedback of the grains transported on the wind itself. More precisely, the flux saturates when the shear velocity inside the reptation layer is so small that the number of reptons promoted to saltation just balances the number of saltons trapped by the sand bed. The most important difference with the previous models comes from the fact that the feedback of the grains on the wind is essentially localized in the reptation layer whereas the sand transport is dominated by saltation.

By comparison with the previous numerical model by Werner (1990), we have shown that the introduction of a complex splash function is inessential as we recover almost the same characteristics with a simple deterministic model. We have reduced the description of the system to a set of two equations governing the evolution in space and time of the reptation and saltation fluxes. The key quantity turns out to be the flux of reptons promoted to saltation. In particular, we have shown that the very long transient before saturation is directly related to a small rate of promotion, even for a moderate reptation flux. The saturation length is found to be slightly

increasing with the wind strength and to be of the order of $7.5–20\rho_{sand}/\rho_{air}d$, which is consistent with field measurements. Finally, we have compared the results of the model to the measurements performed by Rasmussen *et al.* (1996) and Iversen & Rasmussen (1999). The dependencies of the flux and the apparent roughness on the wind strength are correctly described. However, there turns out to be an extra dependence on air viscosity that remains to be explained. This study suggests further experimental measurements to check the existence of two well-separated species and to measure one by one the different parameters of the model.

Appendix. Comparison with experimental measurements

The most precise experiment measuring the saturated flux and the aerodynamic roughness in controlled conditions has been conducted in the Aarhus wind tunnel. We report in figure 12(a) the roughness z_0 rescaled by the Owen prediction $u_*^2/2g$ extracted from figure 7 of Rasmussen *et al.* (1996). The error bars correspond to the statistical dispersion on the original figure. We have shown in figure 5 that the roughness is due to both saltation and reptation and that the velocity reduction inside the reptation layer leads to the presence of a focus. This means that there is a height H_F at which the velocity is U_F whatever u_*. Provided that the wind is almost undisturbed at $z > H_F$, we obtain the relation $U_F = u_* \ln(H_F/z_0)/\kappa$ which can be inverted to give: $z_0 = H_F \exp(-\kappa U_F/u_*)$. If this aerodynamic roughness is smaller than the soil roughness rd, we should recover the latter. This leads to the refined relation:

$$z_0 = H_F \exp\left(-\frac{\kappa U_F}{u_*}\right) + rd. \tag{A 1}$$

We have fitted the experimental data to (A 1) (dotted line on figure 12a) and extracted the parameters H_F, U_F and r. The fit is in reasonable agreement with the data. The height of the focus H_F fixes the amplitude; the velocity at focus U_F determines the position of the curve maximum; the soil roughness rd explains the presence of a minimum on the curves $d = 320\,\mu m$ and $d = 544\,\mu m$. The best fit gives the value $r = 8.5$ which is three times smaller than Bagnold's estimate. We expect the focus height to scale as d and the focus velocity as $\sqrt{gd}$. Unfortunately, both apparently scale as $\sqrt{d}$ (figure 12b). This contradicts the dimensional analysis, meaning that there is an important extra parameter. Most probably it is the air viscosity ν, which allows us to define a timescale t_ν and a lengthscale l_ν:

$$t_\nu = \nu^{1/3}g^{-2/3} \simeq 5.38\,ms, \qquad l_\nu = \nu^{2/3}g^{-1/3} \simeq 284\,\mu m. \tag{A 2}$$

We show in figure 12(b) that $U_F \simeq 1.57\sqrt{\rho_{sand}gd/\rho_{air}}$ and $H_F \simeq 0.53 U_F t_\nu$ are good approximations of the data. We have not found any simple explanation of this scaling with ν. The only indication that we have identified the good parameter is the prefactor of order unity. The solid lines in figure 12a correspond to (A 1) in which H_F and U_F are replaced by their fits in $\sqrt{d}$.

We report in figure 12(c) the total flux rescaled by $\rho_{air}u_*^2\sqrt{d/g}$ as a function of the rescaled shear velocity, extracted from figure 4 of Iversen & Rasmussen (1999). In that case, we were not able to determine error bars. Three important things can be immediately deduced from the figures. First, the threshold velocity is around $4.7\sqrt{gd}$
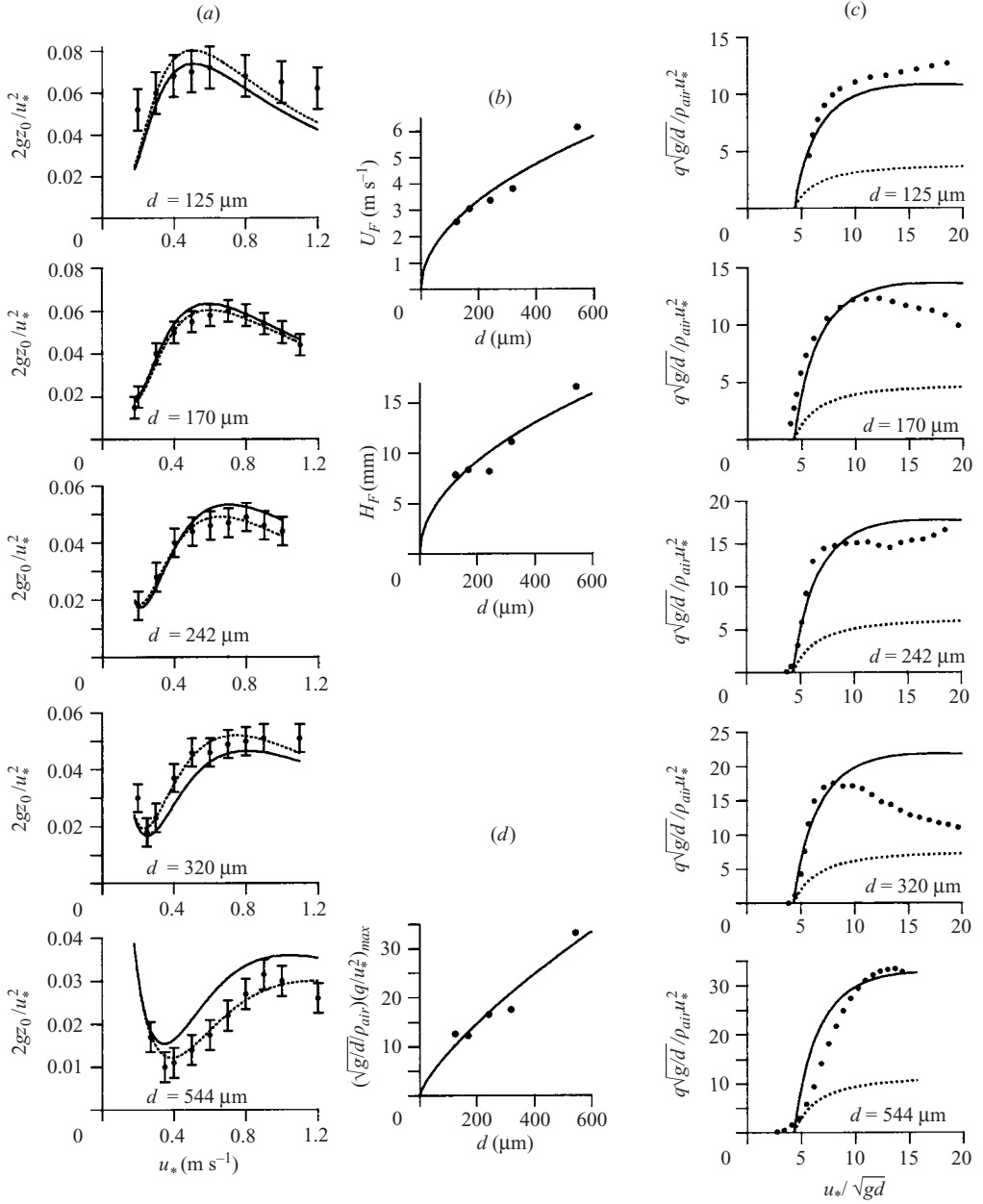
FIGURE 12. (*a*) Rescaled roughness as a function of u_* measured by Rasmussen *et al.* (1996) (black circles). The lines correspond to the relationship expected if there is a focus. The dotted line is the best fit, the parameters of which U_F and H_F are shown on (*b*). The solid lines correspond to U_F and H_F scaling as $\sqrt{d}$. (*c*) Rescaled flux as a function of $u_*/\sqrt{gd}$ measured by Iversen & Rasmussen 1999. The lines correspond to the two-species model (solid line, total flux; dotted line, reptation flux). (*d*) Maximum of the rescaled flux and the scaling in $d^{3/4}$.

which is close to the value obtained in the *n*-generations model for the chosen set of parameters (figure 10). This means that the scaling of u_{th} is good and that a is of the order of 10.

Secondly, the results obtained for different grain sizes do not collapse on a single curve. For instance, the maximum value of the rescaled flux as a function of the grain size d (figure 12d) is obviously not constant. This means again that there is an important extra parameter, probably the air viscosity ν. The solid line in figure 12(d) corresponds to a simple approximation of the data by

$$\left(\frac{q}{u_*^2}\right)_{\text{max}} \simeq 19\rho_{\text{air}}\sqrt{\frac{d}{g}}\left(\frac{d}{l_\nu}\right)^{3/4}.$$

As for the roughness dependence on viscosity, we will not provide any explanation.

Thirdly, we can see that the asymptotic behaviour changes from one grain size to the other. To first order, the flux seems to scale asymptotically as u_*^2 and not as u_*^3 as predicted by Bagnold (1941). Fitting the tails by a power law gives exponents between 1.6 and 2.2. This is quite different from the results of the n-generations model (figure 6) which does not fit the data well as it is. The only parameter on which we can play is the number of ejecta per salton N_{eje}: we have to relax the assumption (2.5) proposed by Werner *et al.* (1990) and McEwan *et al.* 1992. The simplest possibility is to assume, following Ungar & Haff (1987), that a part of the incident energy – and not of the momentum – is restored in the motion of reptons. This argument gives $N_{\text{eje}} \propto v_{\text{imp}}^2/gd$. To model the flux, we have used the equation set (3.7) using the characteristics of saltation and reptation derived from the n-generation model. The lines on figure 12(c) correspond to the parameters

$$\alpha = \left(\frac{d}{l_\nu}\right)^{3/4}, \qquad N_{\text{eje}} = 0.31\left(\frac{v_{\text{imp}}}{a\sqrt{gd}}\right)^2.$$

The agreement with the data is the best that can be done without more information on the parameters of the model. Further work is required to shed light on the dependencies with the viscosity of the surrounding fluid.

REFERENCES

ANDERSON, R. S. & HAFF, P. K. 1988 Simulation of aeolian saltation. *Science* **241**, 820–823.

ANDERSON, R. S. & HAFF, P. K. 1991 Wind modification and bed response during saltation of sand in air. *Acta Mechanica* [Suppl] **1**, 21–51.

ANDERSON, R. S., SØRENSEN, M. & WILLETTS, B. B. 1991 A review of recent progress in our understanding of aeolian sediment transport. *Acta Mechanica* [Suppl] **1**, 1–19.

ANDREOTTI, B., CLAUDIN, P. & DOUADY, S. 2002*a* Selection of barchan shapes and velocities. Part 1: Dynamics of sand, wind and dunes. *Eur. Phys. J.* B **28**, 321–339.

ANDREOTTI, B., CLAUDIN, P. & DOUADY, S. 2002*b* Selection of dune shapes and velocities. Part 2: A two-dimensional modelling. *Eur. Phys. J.* B **28**, 341–352.

BAGNOLD, R. A. 1941 *The Physics of Blown Sand and Desert Dunes*. Chapman and Hall.

CHEPI, W. S. & MILNE, R. A. 1939 Comparative study of soil drifting in the field and in a wind tunnel. *Sci. Agric.* **19**, 149–257.

DOUADY, S., ANDREOTTI, B. & DAERR, A. 1999 On granular surface flow equations. *Eur. Phys. J.* B **11**, 131–142.

GREELEY, R., BLUMBERG, D. G. & WILLIAMS, S. H. 1996 Field measurement of the flux and speed of wind blown sand. *Sedimentology* **43**, 41–52.

HERSEN, P., ANDERSEN, K. H., ELBELRHITI, H., ANDREOTTI, B., CLAUDIN, P. & DOUADY, S. 2004 Corridors of barchan dunes: stability and size selection. *Phys. Rev.* E **69**, 011304.

HERSEN, P., DOUADY, S. & ANDREOTTI, B. 2002 Relevant lengthscale of barchan dunes. *Phys. Rev. Lett.* **89**, 264–301.

IVERSEN, J. D. & RASMUSSEN, K. R. 1994 The effect of surface slope on saltation threshold. *Sedimentology* **41**, 721–728.

IVERSEN, J. D. & RASMUSSEN, K. R. 1999 The effect of wind speed and bed slope on sand transport. *Sedimentology* **46**, 723–731.

JONES, J. R. & WILLETTS, B. B. 1979 Errors in measuring aeolian flow by means of an adjustable trap. *Sedimentology* **26**, 463–468.

KAWAMURA, R. 1951 Study on sand movement by wind. *Rep. Phys. Sci. Res. Inst. of Tokyo University* **5**, 95–112.

KIND, R. J. 1976 A critical examination of the requirements of model simulation of wind induced erosion/deposition phenomena such as snow drifting. *Atmos. Environ.* **10**, 219–227.

LETTAU, K. &. LETTAU, H. H. 1978 Experimental and micro-meteorological field studies of dune migration. In *Exploring the World's Driest Climate* (ed. H. H. Lettau & K. Lettau). University of Wisconsin-Madison, Institute for Environmental studies, IES report vol. 101, pp. 110–147.

MCEWAN, J. K., WILLETTS, B. B. &. RICE, M. A. 1992 The grain/bed collision in sand transport by wind. *Sedimentology* **39**, 971–981.

NALPANIS, P., HUNT, J. C. R. & BARRETT, C. F. 1993 Saltating particles over flat beds. *J. Fluid Mech.* **251**, 661–685 (1993).

NICKLING, W. G. 1978 Eolian sediment transport during dust storms: Slims River valley, Yukon Territory. *Can. J. Earth Sci.* **15**, 1069–1084.

OWEN, P. R. 1964 Saltation of uniform grains in air. *J. Fluid. Mech.* **20**, 225–242.

QUARTIER, L., ANDREOTTI, B., DAERR, A. & DOUADY, S. 2000 Dynamics of a grain on a sandpile model. *Phys. Rev.* E **62**, 8299–8307.

RASMUSSEN, K. R., IVERSEN, J. D. & RAUTAHEIMO, P. 1996 Saltation and wind flow interaction in a variable slope wind tunnel. *Geomorphology* **17**, 19–28.

RIOUAL, F., VALANCE, A. & BIDEAU, D. 2000 Experimental study of the collision process of a grain on a two-dimensional granular bed. *Phys. Rev.* E **62**, 2450–2459.

SAUERMANN, G., KROY, K. & HERRMANN, H. J. 2001 A continuum saltation model for sand dunes. *Phys. Rev.* E **64**, 031305.

SØRENSEN, M. 1985 Estimation of some aeolian saltation transport parameters from transport rate profiles. In *Intl Workshop on the Physics of Blown Sand* (ed. Barndorff-Nielsen, Moller, Rasmussen & Willets), pp. 141–190. University of Aarhus.

SØRENSEN, M. 1991 An analytic model of wind-blown sand transport. *Acta Mechanica* [Suppl] **1**, 67–81.

SVASEK, J. N. & TERWINDT, J. H. J. 1974 Measurements of sand transport by wind on a natural beach. *Sedimentology* **21**, 311–322.

UNGAR, J. E. & HAFF, P. K. 1987 Steady state saltation in air. *Sedimentology* **34**, 289–299.

WERNER, B. T. 1988 The impact process in eolian saltation: two dimensional simulations. *Sedimentology* **35**.

WERNER, B. T. 1990 A steady-state model of wind-blown sand transport. *J. Geol.* **98**, 1–17.

WHITE, B. R. 1979 Soil transport by winds on Mars. *J. Geophys. Res.* **84**, 4643–4651.

WILLETTS, B. B., MCEWAN, J. K. & RICE, M. A. 1991 Initiation of motion of quartz sand grains. *Acta Mechanica* [Suppl] **1**, 123–134.

WILLETTS, B. B., RICE, M. A. & SWAINE, S. E. 1982 Shape effects in aeolian grain transport. *Sedimentology* **29**, 409–417.

WILLIAMS, G. 1964 Some aspects of aeolian saltation load. *Sedimentology* **3**, 257–287.

ZINGG, A. W. 1953 Wind tunnel studies of movement of sedimentary material. *Proc. 5th Hydraulic Conference Bull.* **34**, 111–134.